Nucleon-nucleon cross sections via stochastic processes in phase space: One-dimensional scattering

Sarah John
Eloimagnus Advanced Sciences and Technologies 6701 Democracy Boulevard, Suite 300, Bethesda, Maryland 20817, USA
(Received 3 April 2007; published 11 July 2007)

One-dimensional nucleon-nucleon scattering is simulated by Monte Carlo techniques in the quasiclassical approximation of the Wigner representation. Nucleons are represented by minimum wave packets of approximate nucleon radii, their linear dispersion offset by intrinsic harmonic oscillation, inducing phase space spin in the nucleon Wigner function. A representative set of points evolve in four-dimensional phase space in deterministic classical and stochastic quantum momentum jumps. In the extended space, the inter-nucleon one-pion exchange potential is defined locally by the point coordinates. By the geometric analogy, cross sections are computed from collision distances considered as impact parameters. Results from the parameter free one-dimensional simulation show reasonable agreement with empirical data in the energy range 0.01 GeV to 5 GeV.

DOI: 10.1103/PhysRevC.76.014002 PACS number(s): 21.45.+v, 03.65.Sq, 02.70.Ss, 21.30.−x

I. INTRODUCTION

Nucleon-nucleon cross sections form the fundamental database from which composite nuclear cross sections may be computed. Databases of scattering, fragmentation, fission, and fusion cross sections are not only of profound interest in theoretical nuclear physics, but are gaining increasing technological applications such as in areas of nuclear energy and radiation shielding. Materials evaluation by transport codes based on Boltzmann equation require several types of cross sections. The lack of comprehensive databases is often bridged by theoretical models, of which one notable method is the time-independent phase shift analysis using boson exchange potentials [1–3].

This paper develops a time-dependent method for computation of nucleon-nucleon elastic scattering cross sections [4–8]. The formalism is in the Wigner representation of the quantum Liouville equation (QLE) [9] that has the classical Liouville equation in the limit $\hbar \rightarrow 0$, with higher order terms representing quantum corrections. The development is limited to one-dimensional scattering in the quasiclassical approximation, consisting of the classical and first order quantum terms [10–14].

Solution is by Monte Carlo techniques, with a representative set of phase space points of the Wigner function evolved in deterministic classical trajectories and stochastic quantum momentum jumps in four-dimensional phase space [15]. A unique advantage of the extended four-dimensional phase space is that the potential for each phase space point is defined by its own set of coordinates, the representative set performing its own averaging. This is in contrast to the requirement of a mean potential for simulations in single particle dimensions. Fermi statistics is incorporated by antisymmetrization of the initial state Wigner function, the Hamiltonian conserving the statistics for all times.

Nucleons are represented by minimum wave packets that endow both spatial and momentum distributions to the Wigner function. Wave packet dispersion inherent to linear dynamics is offset by introducing intrinsic harmonic oscillation that in turn induces phase space spin, and hence providing an intuitive physical picture for the hitherto unknown nature of the fermion spin.

The internucleon potential used is the one-pion exchange potential (OPEP) which exhibits a complex range of behavior over isospin, spin, magnetic moment, and tensor variables, together with a core singularity that is either attractive or repulsive. Unlike time-independent solutions based on plane wave expansions, requiring renormalization of the OPEP, for time-dependent simulations using finite width wave packets, the bare OPEP is adequate.

Simulations are performed for repulsive core potentials for backward scattering, enabling computation of an average collision distance equivalent to an energy-dependent impact parameter r_E , from which the total cross section is computed from the geometric formula $\sigma = \pi r_E^2$ [16]. Cross sections computed for the energy range 0.01 GeV to 5 GeV show good trends with empirical data.

The paper is organized as follows: In Sec. II the QLE is antisymmetrized in the Wigner representation, and an initial state Wigner function derived, using minimum wave packet representation for nucleons. Section III discusses solution to the quasiclassical approximation via a stochastic process. Section IV discusses free particle evolution and the necessity of intrinsic harmonic oscillation to maintain fixed spatial widths in free motion. Section V presents the OPEP variables used for the simulations. Section VI presents the results of computed cross sections. Section VII presents some conclusions.

II. ANTISYMMETRIZATION OF PHASE SPACE DYNAMICS

This section derives the Wigner representation for the antisymmetrized QLE, and an initial state Wigner function for two nucleons represented by minimum wave packets.

A. The antisymmetrized QLE

The antisymmetrized QLE is given by (Appendix A)

$$\frac{\partial \hat{\rho}_A}{\partial t} = -i[\hat{H}, \hat{\rho}_A], \tag{1}$$

TABLE I. The comprehensive set of isospin, spin, and m variables for the OPEP.

Isospin	m Isospin	Spin	m		Spatial symmetry
$I = 1$ symmetric	$1, -1, 0$	$S = 1$ symmetric	1	$\uparrow\uparrow$	antisymmetric
	$pp, nn,$		-1	$\downarrow\downarrow$	
	$\frac{1}{\sqrt{2}}(np + pn)$		0	$\frac{1}{\sqrt{2}}(\downarrow\uparrow + \uparrow\downarrow)$	
		$S = 0$ antisymmetric	0	$\frac{1}{\sqrt{2}}(\downarrow\uparrow - \uparrow\downarrow)$	symmetric
$I = 0$ antisymmetric	0	$S = 1$ symmetric	1	$\uparrow\uparrow$	symmetric
	$\frac{1}{\sqrt{2}}(np - pn)$		-1	$\downarrow\downarrow$	
			0	$\frac{1}{\sqrt{2}}(\downarrow\uparrow + \uparrow\downarrow)$	
		$S = 0$ antisymmetric	0	$\frac{1}{\sqrt{2}}(\downarrow\uparrow - \uparrow\downarrow)$	antisymmetric

where A is the antisymmetrization operator, $\hat{\rho}$ the density operator, $\hat{H}$ is the Hamiltonian, and

$$\hat{\rho}_A = A\hat{\rho}A^* = |\Psi_A\rangle\langle\Psi_A|, \tag{2}$$

with the antisymmetrized state $|\Psi_A\rangle$ defined by

$$|\Psi_A\rangle = A|\Psi\rangle, \tag{3}$$

where $|\Psi\rangle$ is the product wave function of isospin, spin and spatial wave functions, the symmetry requirements for each specified in Table I.

With the Wigner transform of an operator $\hat{O}(t)$ defined by

$$O_w(x, p, t) = \int_{-\infty}^{\infty} dy\, e^{ip\cdot y}\left\langle x - \frac{1}{2}y\right|\hat{O}(t)\left|x + \frac{1}{2}y\right\rangle \tag{4}$$

the Wigner transform of the antisymmetrized QLE is

$$\frac{\partial f_w^A}{\partial t}(x, p, t) = -2H_w \sin\left(\frac{\Lambda}{2}\right) f_w^A(x, p, t), \tag{5}$$

where (x, p) are each six component variables, f_w^A is the antisymmetrized Wigner function defined by

$$f_w^A(x, p, t) = \frac{1}{C}\int_{-\infty}^{\infty} dy\, e^{ip\cdot y}\left\langle x - \frac{1}{2}y\right|\hat{\rho}_A\left|x + \frac{1}{2}y\right\rangle \tag{6}$$

with normalization

$$C = \int_{-\infty}^{\infty} dxdpdy\, e^{ip\cdot y}\left\langle x - \frac{1}{2}y\right|\hat{\rho}_A\left|x + \frac{1}{2}y\right\rangle \tag{7}$$

and the Poisson operator defined by

$$\Lambda = \overleftarrow{\nabla}_p \cdot \overrightarrow{\nabla}_x - \overleftarrow{\nabla}_x \cdot \overrightarrow{\nabla}_p \tag{8}$$

the arrows directed to the function it operates on.

B. Nucleon-nucleon Wigner function

Nucleons are represented by wave packets obeying minimum uncertainty relations, as the one given by [17]

$$\psi_1(x_1) = \pi^{-\frac{1}{4}} e^{-\frac{(x_1 - \bar{x}_1)^2}{2} - i\bar{p}_1 x_1}, \tag{9}$$

where subscripts on dynamical variables indicate the particle type, while those on expectation values $(\bar{x}_1, \bar{p}_1)$ define the subscript on the wave function. A second wave packet is defined by the subscript 2. The above form obeys the minimum uncertainty relation $\Delta x \cdot \Delta p = 1/2$ with $\hbar = 1$. The spatial half-width, obtained from $\psi\psi^*$, is

$$\sigma = 1/\sqrt{2} = 0.707 \tag{10}$$

which is a good approximation to the nucleon radius of 0.86 fm. The given form however is retained for simpler algebra and symmetric form for spatial and momentum distributions of the Wigner function.

The symmetrized/antisymmetrized spatial wave function for the two minimum wave packets is

$$\psi_\pm(x_1, x_2) = \frac{1}{\sqrt{2}}(\psi_1(x_1)\psi_2(x_2) \pm \psi_1(x_2)\psi_2(x_1))\cdot \tag{11}$$

Substituting in the two-particle Wigner function defined by

$$\begin{aligned} f_w(\vec{x}_1, \vec{p}_1, \vec{x}_2, \vec{p}_2, t) &= \frac{1}{C}\int_{-\infty}^{\infty} d\vec{y}_1 d\vec{y}_2\, e^{i(\vec{p}_1\cdot\vec{y}_1 + \vec{p}_2\cdot\vec{y}_2)} \\ &\times \left\langle \vec{x}_1 + \frac{1}{2}\vec{y}_1, \vec{x}_2 + \frac{1}{2}\vec{y}_2\right|\psi(t)\Big\rangle \\ &\times \left\langle \psi(t)\left|\vec{x}_1 - \frac{1}{2}\vec{y}_1, \vec{x}_2 - \frac{1}{2}\vec{y}_2\right\rangle\right. \end{aligned} \tag{12}$$

obtains after a lengthy but straightforward algebra

$$\begin{aligned} f_w^{\pm}(x_1, p_1, x_2, p_2) &= \frac{1}{C}\big[f_w^1(x_1, p_1, x_2, p_2) + f_w^2(x_2, p_2, x_1, p_1) \\ &\quad \pm 4e^{-\frac{1}{2}(x^2+p^2)}e^{-2((X-\bar{X})^2+(P-\bar{P})^2)} \\ &\quad \times \cos(2(X\bar{p} - P\bar{x}))\big], \end{aligned} \tag{13}$$

where the $\pm$ term is the exchange term, and

$$\begin{aligned} f_w^1(x_1, p_1, x_2, p_2) &= e^{-(x_1-\bar{x}_1)^2-(p_1-\bar{p}_1)^2} \\ &\quad \times e^{-(x_2-\bar{x}_2)^2-(p_2-\bar{p}_2)^2}, \\ f_w^2(x_2, p_2, x_1, p_1) &= e^{-(x_2-\bar{x}_1)^2-(p_2-\bar{p}_1)^2} \\ &\quad \times e^{-(x_1-\bar{x}_2)^2-(p_1-\bar{p}_2)^2}, \end{aligned} \tag{14}$$

where

$$\begin{aligned} \bar{X} &= \tfrac{1}{2}(\bar{x}_1 + \bar{x}_2), \quad X = \tfrac{1}{2}(x_1 + x_2), \\ \bar{x} &= \bar{x}_1 - \bar{x}_2, \quad x = x_1 - x_2, \end{aligned} \tag{15}$$

$$\begin{aligned} \bar{P} &= \tfrac{1}{2}(\bar{p}_1 + \bar{p}_2), \quad P = \tfrac{1}{2}(p_1 + p_2), \\ \bar{p} &= \bar{p}_1 - \bar{p}_2, \quad p = p_1 - p_2. \end{aligned} \tag{16}$$

The normalization constant is

$$C = 4\pi^2 \pm 2\pi^2 e^{-\frac{1}{2}(\bar{x}^2+\bar{p}^2)}\cos(2(\bar{X}\bar{p} + \bar{x}\bar{P})) \tag{17}$$

with the $\pm$ corresponding to the exchange term of Eq. (13).

Figure 1(a) shows the Wigner function for nucleons well separated in space and momentum. The figures are projections from four-dimensions to two-dimensions by integrating over second particle coordinates. The exchange term is significant only when both spatial and momentum coordinates overlap simultaneously as shown in Fig. 1(b) for the symmetrized function, and in Fig. 1(c) for the antisymmetrized function. Figure 2 is the contour plot of Fig. 1(c).

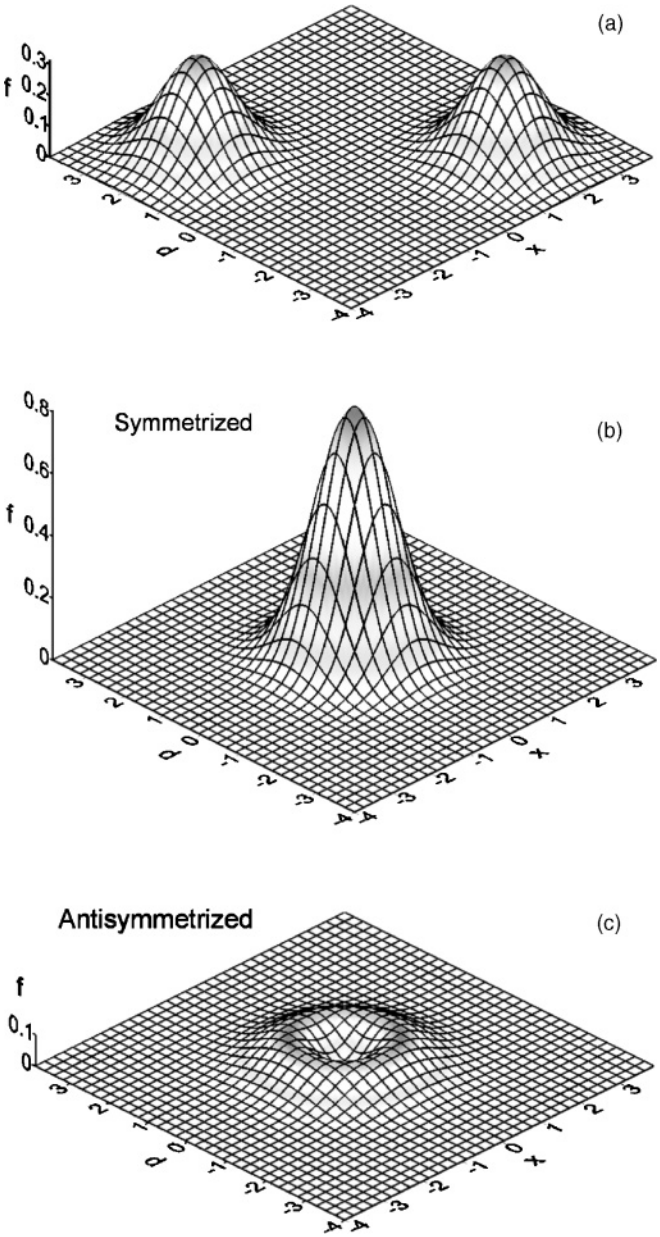

FIG. 1. (a) Wigner function for nucleons well separated in space and momentum with $(\bar{x}, \bar{p})$ at $(2, -2)$ and $(-2, 2)$ for the two wave packets, (b) for symmetrized function with $(\bar{x}, \bar{p})$ at $(0.25, -0.25)$, and $(-0.25, 0.25)$, and (c) the corresponding antisymmetrized function.

III. SOLUTION VIA STOCHASTIC PROCESS

The two-particle Hamiltonian is given by

$$H = \sum_{i=1,2} \frac{p_i^2}{2m_i} + V(|x_1 - x_2|), \tag{18}$$

where i is the particle and V the one-pion exchange potential.

The solution of Eq. (5) to order $O(\Delta t^2)$ written as

$$f_w^A(x, p, t + \Delta t) = e^{-L_q \Delta t} e^{-L_c \Delta t} f_w^A(x, p, t) + O(\Delta t^2) \tag{19}$$

expresses evolution in incremental sequential classical and quantum steps, the classical step according to the classical Liouville equation,

$$\frac{\partial f_w(x, p, t)}{\partial t} = -L_c f_w(x, p, t) = -\{H_w, f_w\}, \tag{20}$$

where $\{\}$ denotes the Poisson bracket, and the quantum step according to

$$\frac{\partial f_w(x, p, t)}{\partial t} = -L_q f_w(x, p, t) \tag{21}$$

with the quantum operator for one-dimensional scattering given by

$$\begin{aligned} L_q &= \tfrac{1}{24}(\partial_{x_1}\partial_{p_1} + \partial_{x_2}\partial_{p_2})^3 V(|x_1 - x_2|) \\ &= \tfrac{1}{24} V'''_{x_1}(\partial_{p_1} - \partial_{p_2})^3 \end{aligned} \tag{22}$$

in the quasiclassical approximation.

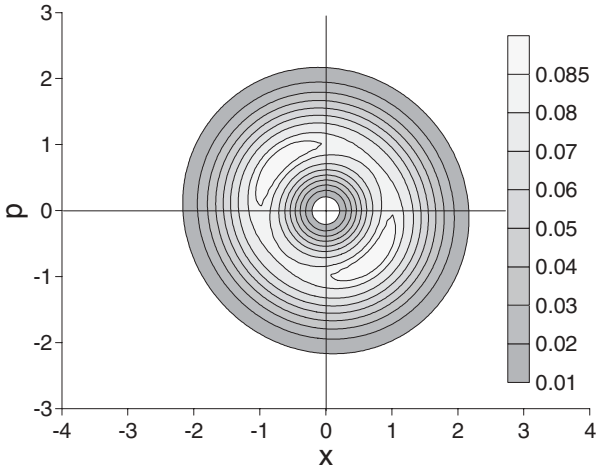

FIG. 2. Contour plot of Fig. 1(c) for the antisymmetrized Wigner function.

A. Monte Carlo solution

A representative set for the initial state Wigner function is given by four-dimensional phase space points,

$$f_w(x_1, p_1, x_2, p_2, 0) \approx \frac{1}{N}\sum_{j=1}^{N}\sigma_j \delta(x_1 - x_{1j})\delta(p_1 - p_{1j}) \times \delta(x_2 - x_{2j})\delta(p_2 - p_{2j}), \quad (23)$$

where σ_j is the sign of the function at the phase space point, and N the number of sample points.

The classical evolution of a phase space point at $(x_{1j}, p_{1j}, x_{2j}, p_{2j})$ is by the Hamilton equations of motion,

$$\frac{\partial p_{ij}}{\partial t} = -\frac{\partial H_w}{\partial x_{ij}}, \quad \frac{\partial x_{ij}}{\partial t} = \frac{\partial H_w}{\partial p_{ij}}, \quad (24)$$

evolving the point in a deterministic trajectory.

Changing the variables of the quantum operator given by Eq. (22) to

$$\begin{aligned} v_1 &= p_1 + p_2, \\ v_2 &= p_1 - p_2 \end{aligned} \quad (25)$$

obtains

$$L_q = \tfrac{1}{3} V'''_{x_1} \partial^3_{v_2} \quad (26)$$

together with the transformation

$$\delta(p_1 - p_{1j})\delta(p_2 - p_{2j}) \to 2\delta(v_1 - v_{1j})\delta(v_2 - v_{2j}), \quad (27)$$

where 2 is the Jacobian of the transformation. The quantum evolution of the momentum delta functions is therefore

$$e^{-(a_j/8)(\partial_{p_1} - \partial_{p_2})^3}\delta(p_1 - p_{1j})\delta(p_2 - p_{2j}) \to 2e^{-a_j \partial^3_{v_2}}\delta(v_1 - v_{1j})\delta(v_2 - v_{2j}), \quad (28)$$

where

$$a_j = \Delta t\, V'''_{x_{1j}}/3. \quad (29)$$

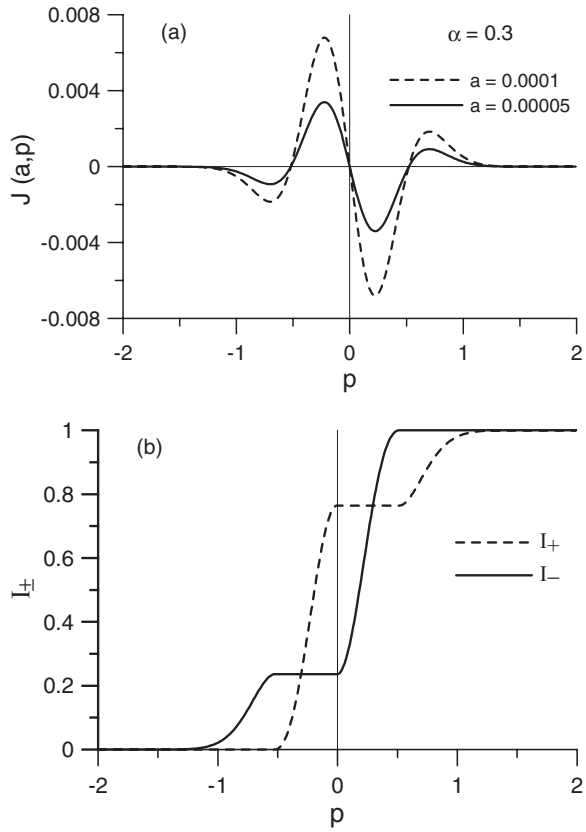

FIG. 3. (a) The jump function and (b) the positive and negative cumulative distribution which is identical to both curves shown in (a).

The quantum evolution transforms $\delta(v_2 - v_{2j})$ into an Airy function with slowly decaying oscillations. To achieve faster damping, the delta function is smoothed into a gaussian function $\delta_\alpha(v_2 - v_{2j})$ of variance α^2. The jump function defined by

$$J_\alpha(a_j, v_2 - v_{2j}) = e^{-a_j \partial^3_{v_2}}\delta_\alpha(v_2 - v_{2j}) - \delta_\alpha(v_2 - v_{2j}) \quad (30)$$

is plotted in Fig. 3(a) for $\alpha = 0.3$, using a series expansion with Hermite polynomials, which is valid for $a_j/\alpha^3 \ll 1$ [14].

With the area under the positive and negative regions of the jump function equal and given by

$$A_j = \int_{-\infty}^{\infty} |J_+| dp = \int_{-\infty}^{\infty} |J_-| dp, \quad (31)$$

where $J_\pm$ represent the positive and negative values of the function, one may write

$$\begin{aligned} J_\alpha(a_j, v_2 - v_{2j}) &= A_j \left(\frac{|J_+|}{A_j} - \frac{|J_-|}{A_j} \right) \\ &= P(A_j)(P(p_+|A_j) - P(p_-|A_j)), \end{aligned} \quad (32)$$

where $P(A_j) = A_j$ is the probability for a stochastic jump and the conditional probabilities defined by

$$P(p_+|A_j) = \frac{|J_+|}{A_j}, \quad P(p_-|A_j) = \frac{|J_-|}{A_j} \quad (33)$$

selects a pair of positive and negative points with momentum p_+ and p_-, respectively, the process equivalent to a first order Markov process. A procedure for implementing the conditional probabilities is by the cumulative distribution, defined by

$$\begin{aligned} I_+(p) &= \int_{-\infty}^{p} P(p_+|A_j)dp_+, \\ I_-(p) &= \int_{-\infty}^{p} P(p_-|A_j))dp_- \end{aligned} \tag{34}$$

shown in Fig. 3(b). For $a_j/\alpha^3 \ll 1$ the cumulative distribution is identical for all a, whereas the area increases linearly as

$$A_j = m_\alpha a_j, \tag{35}$$

where m_α is the slope. The Markov process indicates that not all phase space points undergo quantum events, but only those selected randomly with probability $P(A_j)$, in which case a single pair of positive and negative points are created by conditional probabilities. For a large density of points, this procedure effectively obtains a representative set for the jump function.

Even with the above procedure, creation of new points can rapidly overwhelm computing resources. Therefore, a simple algorithm is proposed. Note from Fig. 3(b) that the cumulative probability for the negative point is approximately one-fourth along the negative p axis and three-fourths along the positive p axis, and vice versa for the positive point. Computing the root mean square momentum for the positive and negative lobes on each side, an algorithm for the jump function is

$$\begin{aligned} J_\alpha(a_j, v_2 - v_{2j}) &= P(A_j)(-P_1(-\eta_1) + P_2(-\eta_2) \\ &\quad - P_3(\eta_3) + P_4(\eta_4)) \end{aligned} \tag{36}$$

with probabilities and momentum coordinates for a created pair having only four possibilities relative to the parent point, as given by

$$\begin{aligned} P_1(-\eta_1) &= \frac{1}{4}, \quad P_2(-\eta_2) = \frac{3}{4}, \quad P_3(\eta_3) = \frac{3}{4}, \\ P_4(\eta_4) &= \frac{1}{4}, \quad \eta_1 = \left(\int_{-\infty}^{0} dp_- p_-^2 P(p_-|A_j)\right)^{1/2}, \\ \eta_2 &= \left(\int_{-\infty}^{0} dp_+ p_+^2 P(p_+|A_j)\right)^{1/2}, \\ \eta_3 &= \left(\int_{0}^{\infty} dp_- p_-^2 P(p_-|A_j)\right)^{1/2}, \\ \eta_4 &= \left(\int_{0}^{\infty} dp_+ p_+^2 P(p_+|A_j)\right)^{1/2}. \end{aligned} \tag{37}$$

An immediate annihilation process may be considered with the outermost pairs annihilating one inner pair, resulting in

$$\begin{aligned} J_\alpha(a_j, v_2 - v_{2j}) &= P(A_j)(P_2'(-\eta_2) - P_3'(\eta_3))), \\ P_2'(-\eta_2) &= \tfrac{1}{2}, \quad P_3'(\eta_3) = \tfrac{1}{2}. \end{aligned} \tag{38}$$

One may now interpret the conditional probability as a certain pair creation, creating a positive point with momentum $-\eta_2/2$, and a negative point with momentum $\eta_3/2$ in time interval Δt, instead of a pair at $(-\eta_2, \eta_3)$ at half probability. Over time $2\Delta t$ the former may be a better approximation when annihilations are considered. Annihilating the positive parent with the negative point is then equivalent to an effective momentum jump for the parent obtaining

$$J_\alpha(a_j, v_2 - v_{2j}) = P(A_j)\left(\delta\left(v_2 - (v_{2j} - \tfrac{1}{2}\eta_2\right)\right). \tag{39}$$

Such stochastic jumps when applied to all points, however, looses the capacity to generate negative regions, but presents a significantly faster algorithm. Transforming back to the original coordinates via

$$\begin{aligned} \Delta v_1 &= 0 \rightarrow \Delta p_1 = -\Delta p_2, \\ \Delta v_2 &= -\tfrac{1}{2}\eta_2 = 2\Delta p_1, \end{aligned} \tag{40}$$

obtains the representation for the jump function in the original coordinates (the factor 2 in Eq. (28) canceling with the Jacobian 1/2 of the inverse transformation) to be

$$\begin{aligned} J &= P(A_j)\delta\left(p_1 - \left(p_{1j} - \tfrac{1}{4}\eta_2\right)\right) \\ &\quad \times \delta\left(p_2 - \left(p_{2j} + \tfrac{1}{4}\eta_2\right)\right). \end{aligned} \tag{41}$$

This algorithm is simple to implement and fast in execution, and was found to give good results when applied to the example of the quartic potential in Refs. [13,14], and from which an approximate optimal value of $\alpha = 0.3$ was determined that obtains

$$m_\alpha = 27.9, \quad \eta_1 = \eta_4 = 0.38, \quad \eta_2 = \eta_3 = 0.23. \tag{42}$$

IV. FREE-PARTICLE MOTION: PHASE SPACE SPIN

Free particle evolution is considered first to demonstrate the incompatibility of wave packet representation for linear dynamics, as it spreads the spatial width over time. To achieve meaningful simulation of fixed width nucleons, a novel concept of internal harmonic oscillation is introduced, which by inducing phase space spin of the Wigner function preserves spatial width.

Figure 4(a) shows the initial state Wigner function for wave packets well separated in phase space. The free particle Hamiltonian

$$H_0 = \sum_i \frac{p_i^2}{2m_i} \tag{43}$$

propagates each point classically according to

$$\frac{\partial x_{ij}}{\partial t} = \frac{p_{ij}}{m_i}, \quad \frac{\partial p_{ij}}{\partial t} = 0, \tag{44}$$

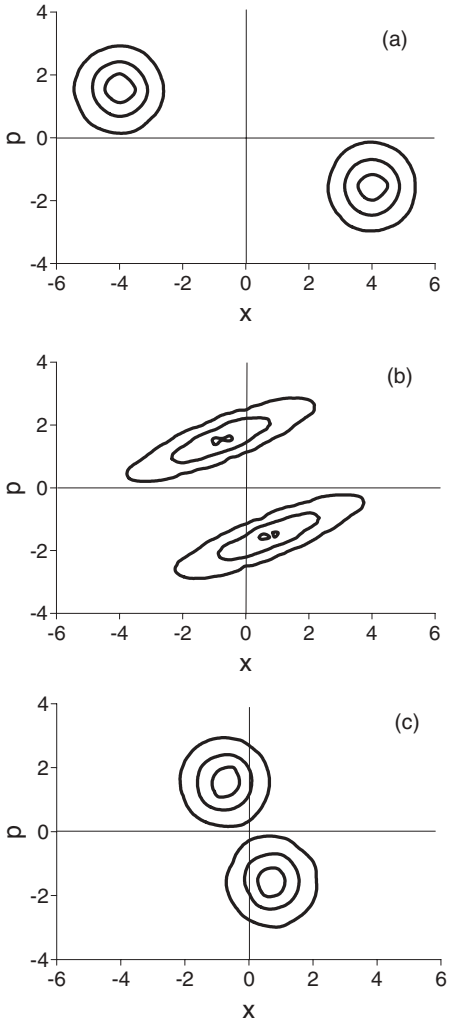

FIG. 4. Free particle evolution, (a) initial state, (b) evolution showing dispersion, (c) evolution with phase space spin.

resulting in the state shown in Fig. 4(b) after a finite time interval. Wave packet spreading is severe, indicating that wave packets are a poor representation for fixed radius nucleons in linear dynamics.

A novel way to offset dispersion is by introducing internal harmonic oscillation to the free particle Hamiltonian as given by

$$H_0 = \sum_i \frac{p_i^2}{2m_i} + \sum_i \int \frac{(x_i' - \langle x_i \rangle)^2}{2m_i} \rho(x_i') dx_i', \qquad (45)$$

where $\rho(x_i) = |\psi(x_i)|^2$ are single particle densities. Note for point particles this term is zero. The equations of motion is now given by

$$\frac{\partial x_{ij}}{\partial t} = s_i \frac{p_{ij}}{m_i}, \quad \frac{\partial p_{ij}}{\partial t} = -s_i \frac{x_{ij} - \langle x_i \rangle}{m_i}, \qquad (46)$$

inducing a rotation or phase space spin about the average $\langle x_i \rangle$ for the single particle Wigner function. The factor $s_i = \pm 1$ corresponds to clockwise and anticlockwise rotations, $s_i = -1$ reversing initial momentum, as well as quantum jumps.

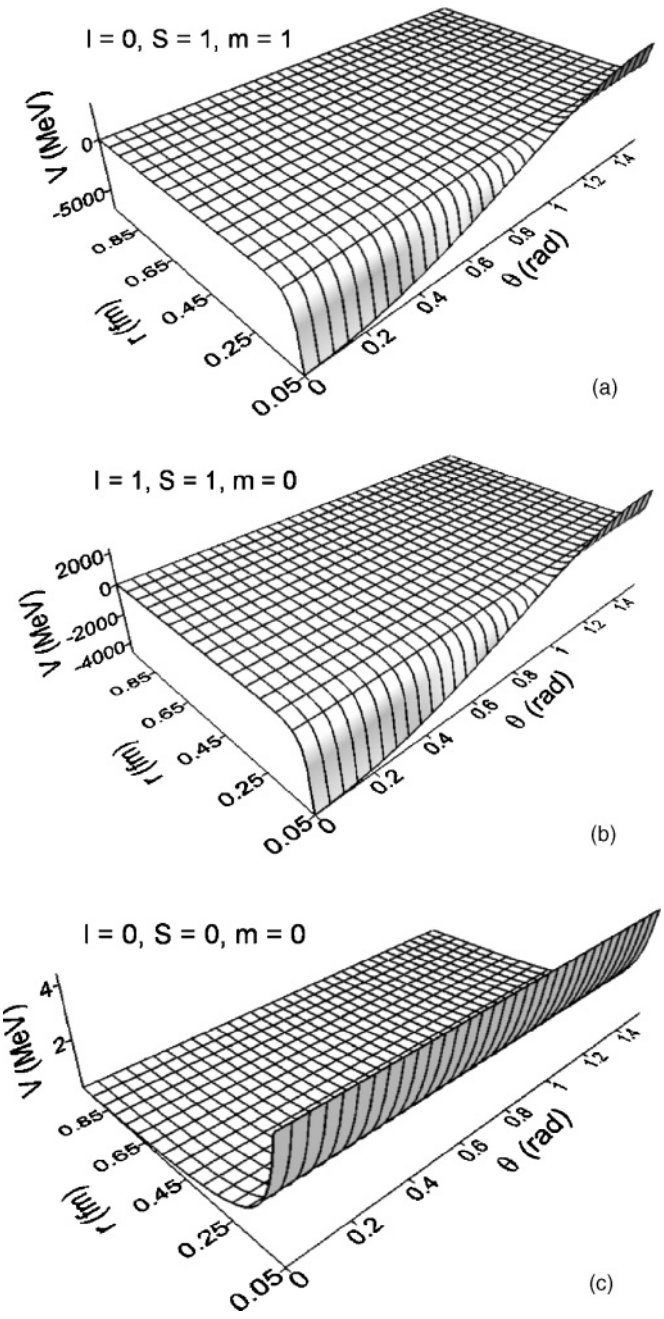

FIG. 5. The 3D graphs of potentials used for simulations, presenting a repulsive core for spin orientations $\theta_c < \theta \leqslant \pi/2$.

Evidently, free particle evolution now preserves both spatial and momentum widths perfectly as shown in Fig. 4(c).

The harmonic term may be considered an effective method to preserve widths, obviating more complicated internal forces. As its range is confined to within wave packet dimensions, internucleon interactions are not modified, although a residual effect is observed between clockwise and anticlockwise spins. On the other hand, it provides an intuitive picture of a spinning nucleon and a justification for the spin 1/2 states in the form of clockwise and anticlockwise rotations of nucleon Wigner functions in phase space.

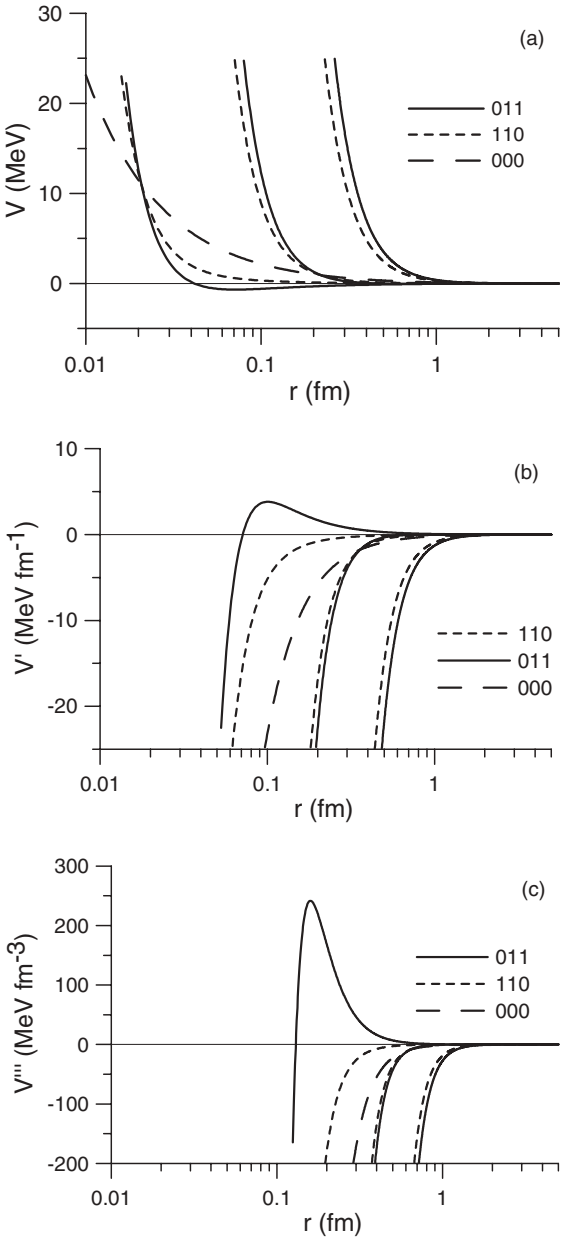

FIG. 6. (a) Potentials for orientations of $\theta = \pi/2$, $\theta = \theta_c + 0.01$, and $\theta = \theta_c + 0.0001$ in that order from right to left for (1,1,0), (0,1,1), and for the θ independent (0,0,0), (b) the corresponding first derivatives, and (c) the corresponding third derivatives.

V. THE ONE-PION EXCHANGE POTENTIAL

The one-pion exchange potential (OPEP) is given by

$$V(r) = \frac{g^2}{4\pi}\frac{m_\pi^2}{12m_N^2}(\tau_1\cdot\tau_2)\left\{\underbrace{\sigma_1\cdot\sigma_2}_{\text{central}}\frac{e^{-\mu_\pi r}}{r} + \underbrace{(3\sigma_1\cdot\hat{r}\sigma_2\cdot\hat{r}-\sigma_1\cdot\sigma_2)}_{\text{tensor}}\frac{e^{-\mu_\pi r}}{r} \times\left(1+\frac{3}{\mu_\pi r}+\frac{3}{(\mu_\pi r)^2}\right)\right\}, \quad (47)$$

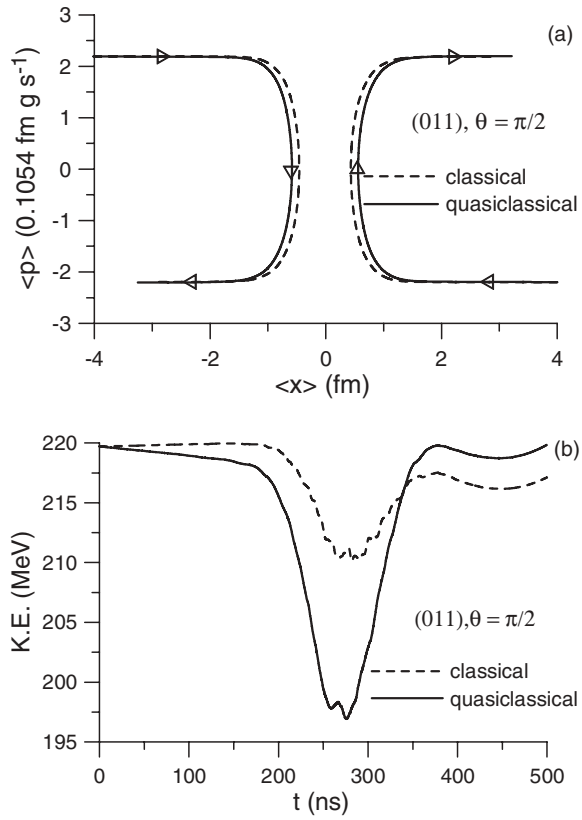

FIG. 7. Simulations for (0,1,1) for $\theta = \pi/2$, (a) $\langle x\rangle$ vs $\langle p\rangle$ and (b) total kinetic energy vs time.

where $r = |x_1 - x_2|$, m_π and m_N are the masses of the pion and the nucleon, respectively, $\mu_\pi = m_\pi/\hbar c$, τ and σ are the isospin and spin of the nucleon, and $g^2/4\pi \approx 0.07$ for meson exchange, and $\sigma_1\cdot\sigma_2 = 1$ for $S = 1$ and $\sigma_1\cdot\sigma_2 = -3$ for $S = 0$. Similarly $\tau_1\cdot\tau_2 = 1$ for $I = 1$ and $\tau_1\cdot\tau_2 = -3$ for $I = 0$, where S is the total spin, and I the total isospin.

The tensor component can be simplified as follows:

$$(\sigma_1\cdot\hat{r})(\sigma_2\cdot\hat{r}) = \begin{cases}\cos^2\theta & S=1, m=1\\ \cos^2\theta & S=1, m=-1\\ \cos^2\theta-\sin^2\theta & S=1, m=0\\ -1 & S=0, m=0\end{cases}, \quad (48)$$

where θ is the spin orientation of each nucleon along r, and m is the projection.

The 3D graphs of potentials used for the simulations are shown in Fig. 5 as a function of spin orientation and distance r, and correspond to the set (I, S, m) of (0,0,0), (1,1,0) and (0,1,1). Simulations are performed for orientations $\theta_c < \theta \leqslant \pi/2$, where θ_c corresponds to the fermion spin quantization $m = 1/2$ is given by $\cos\theta_c = 1/\sqrt{3}$, and is the turning point from attractive to repulsive cores. Figure 6(a) shows the 2D plots for orientations of $\theta = \pi/2$, $\theta = \theta_c + 0.01$, and $\theta = \theta_c + 0.0001$ in that order from right to left for (1,1,0) and (0,1,1) with the (0,0,0) potential being θ independent. The corresponding first derivatives are shown in Fig. 6(b), and the third derivatives in Fig. 6(c). These

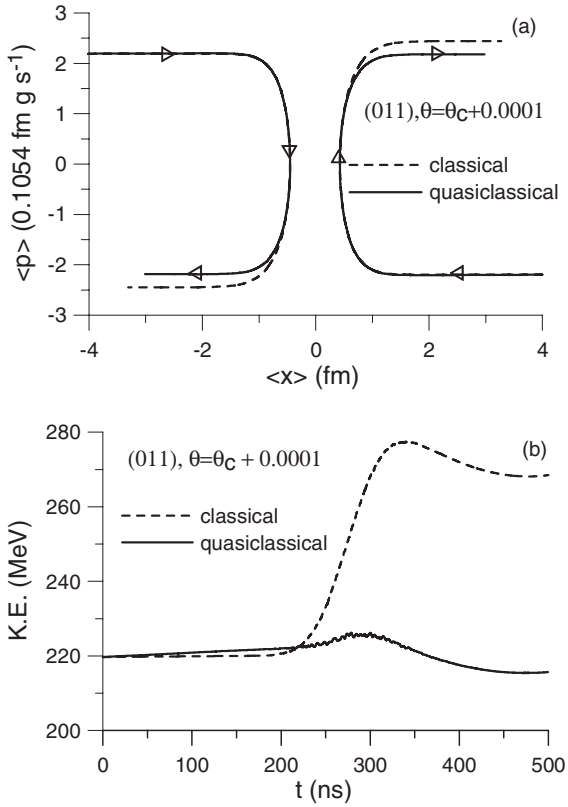

FIG. 8. Simulations for (0,1,1) for $\theta = \theta_c + 0.0001$, (a) $\langle x \rangle$ vs $\langle p \rangle$ and (b) total kinetic energy vs time.

derivatives play a role in the classical and quantum evolutions, respectively.

VI. CROSS SECTIONS

The geometric cross section is given by $\sigma = \pi r_E^2$, where r_E is the energy-dependent impact parameter between centers of interacting nucleons. The formula may be extended to one-dimensional back scattering by interpreting the collision distance to be equivalent to an impact parameter.

Simulations were performed for potentials presenting a repulsive core to attain back scattering. A unique advantage of the extended four dimensional phase space is that the potential for each phase space point is defined by its own set of coordinates, the representative sample set performing averaging. This is in contrast to the use of a mean field potential for simulations in single particle spatial dimension.

The program, written in C was run on a Pentium 4 desktop computer. List processing techniques were used that enable evolutionary increments of phase space coordinates to arbitrary accuracy, unlike the limitation of grid spacing. The initial spatial distance between the wave packets was set at 8 fm and simulations were performed in the center of mass frame for lab energy varying between 0.01 GeV to 5 GeV. The initial state Wigner function was represented by 5×10^3 phase space points for general runs. The execution time was fast, not exceeding 2 min for a single energy run that is terminated at the minimum collision distance.

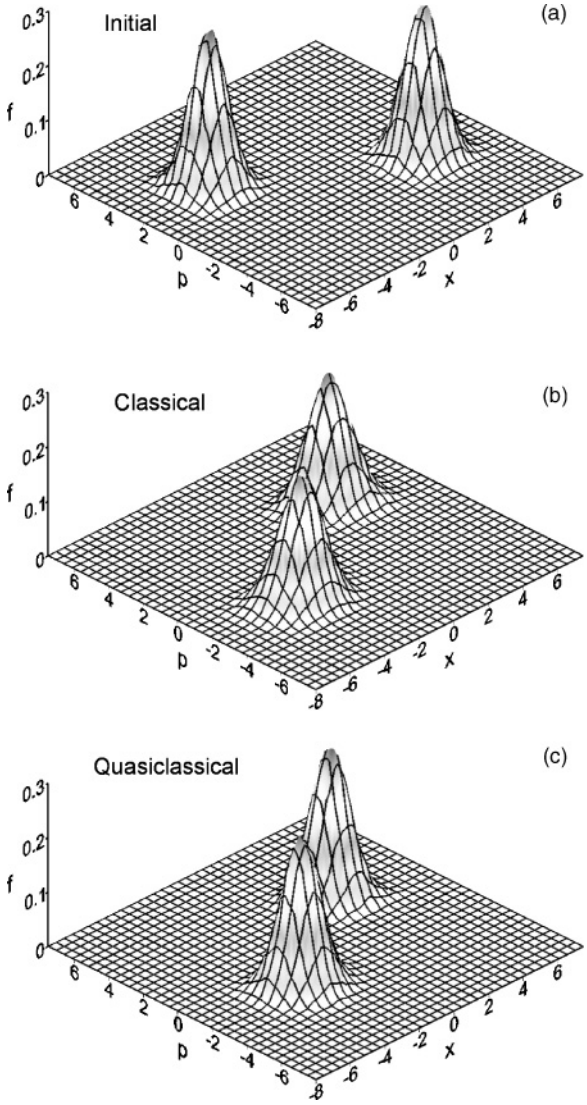

FIG. 9. The single particle Wigner functions for (a) initial state (b) classical evolution and (c) quasiclassical evolution at the end time of Fig. 8(b).

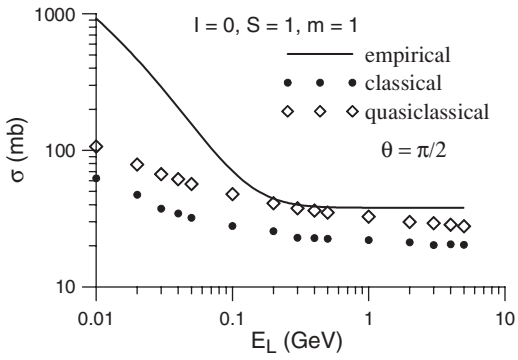

FIG. 10. Computed cross sections from classical and quasiclassical evolutions, compared with the empirical neutron-proton total cross sections.

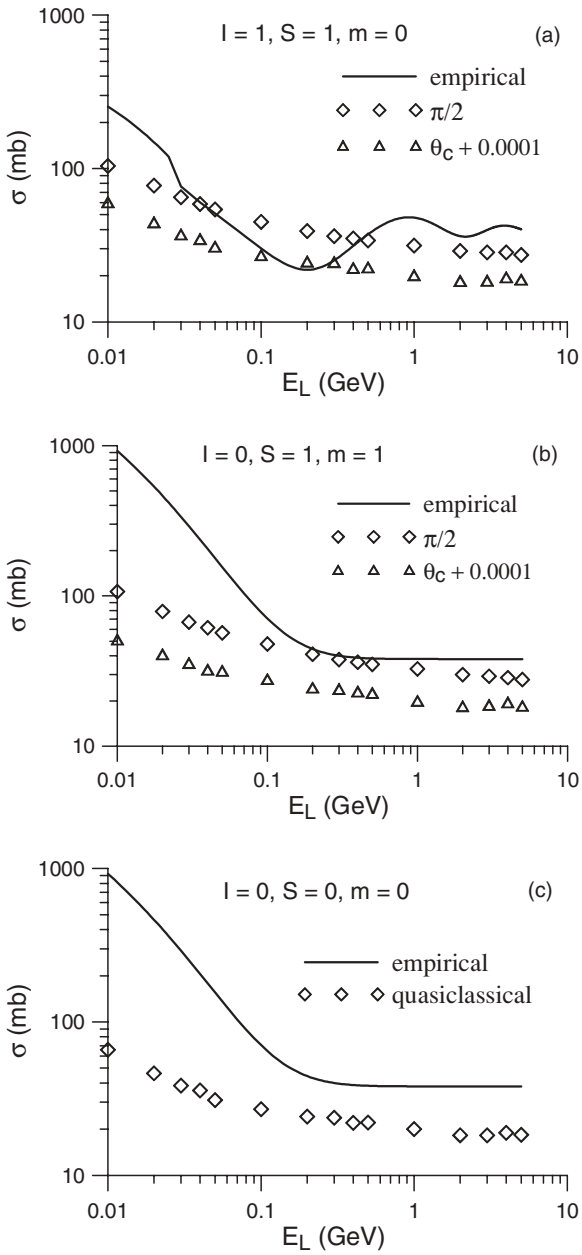

FIG. 11. Computed cross sections from quasiclassical evolution for (a) (1,1,0) compared with empirical proton-proton cross sections, (b) (0,1,1) compared with empirical neutron-proton cross sections, and (c) (0,0,0) compared with empirical neutron-proton cross sections.

Figures 7–9 correspond to simulations for (0,1,1) continued well beyond the collision distance. Averages and the total kinetic energy are computed from the phase space point coordinates. The total kinetic energy includes the lab energy plus the internal energy of each particle due to finite momentum distribution. Plots for $\langle x \rangle$ vs. $\langle p \rangle$ and total kinetic energy vs time are shown in Figs. 7 and 8. Figure 7 corresponds to $\theta = \pi/2$, for which the potential is entirely repulsive, and Fig. 8 for $\theta = \theta_c + 0.0001$ corresponds to a potential with a shallow attractive well and repulsive core. For $\theta = \pi/2$, both classical and quasiclassical evolutions are seen to conserve energy and momentum. However, for the $\theta = \theta_c + 0.0001$, the quasiclassical simulation presents the true dynamics, conserving both momentum and energy, compared to the classical evolution. Figure 9 shows the single particle Wigner functions for (a) the initial state, (b) classical evolution and (c) quasiclassical evolution at the end time of Fig. 8(b).

Figure 10 shows the computed cross sections for both the classical and quasiclassical evolutions for (0,1,1) at $\theta = \pi/2$. For comparison the empirical neutron-proton total cross sections is also plotted [18].

Figure 11 shows the computed cross sections from quasiclassical evolution, for (1,1,0), (0,1,1), and (0,0,0). Figure 11(a) for (1,1,0) pertains to proton-proton, neutron-neutron, neutron-proton scattering (see Table I). The empirical curve for proton-proton total cross section shows good agreement with the simulation results.

Figure 11(b) for (0,1,1) pertains to exclusive neutron-proton scattering, and is compared with the empirical neutron-neutron curve. The simulation data follow closely the empirical trend. Quantitative differences, particularly at high energy, may be attributed to the approximations used in the wave packet half-width of 0.707 fm rather than nucleon radius of 0.86 fm, and lower energy discrepancies may be attributed to limitations of one-dimensional scattering, and to variations in the running coupling constant.

Figure 11(c) for (0,0,0) corresponds to isospin and spin singlet, spin up-spin down case pertaining to exclusive neutron-proton scattering. The potential being independent of θ results in a unique set of cross sections.

VII. CONCLUSIONS

Nucleon-nucleon dynamics in the Wigner representation is simulated in the quasiclassical approximation in the one-pion exchange potential by Monte Carlo techniques. Nucleons are represented by wave packets of half-widths approximately equal to the nucleon radius, with linear dispersion offset by internal harmonic oscillation, inducing phase space spin to the nucleon Wigner function. Cross sections computed from the geometric analogy for total cross sections, using minimum collision distances as equivalent to impact parameters, show satisfactory agreement with empirical curves.

This study suggests that extensions to two- and three-dimensional scattering in 8- and 12-dimensional phase space, respectively, is viable for computation of differential cross section, resulting in a more accurate evaluation of the total cross section.

ACKNOWLEDGMENTS

This work was supported in part by NASA contract No. NNL05AB03P.

APPENDIX

The N particle linear symmetrizing/antisymmetrizing operators are defined by

$$S = \frac{1}{\sqrt{N!}} \sum_i P_i$$

and

$$A = \frac{1}{\sqrt{N!}} \sum_i \pm P_i,$$

respectively, where P_i is an element of the permutation group. For the antisymmetrizing operator the + and − sign are assigned to P_i even and odd, respectively. For example, the two-particle permutation group is $\{1, P_{12}\}$ where the permutation element P_{12} exchanges the particles, obtains

$$S = \tfrac{1}{\sqrt{2}}(1 + P_{12}), \quad A = \tfrac{1}{\sqrt{2}}(1 - P_{12}).$$

that applied to the two-particle spatial wave function

$$\psi(x_1, x_2) = \psi_1(x_1)\psi_2(x_2)$$

obtains the symmetrized state

$$\begin{aligned} \psi_s(x_1, x_2) &= S\psi_s(x_1, x_2) \\ &= \tfrac{1}{\sqrt{2}} \left(\psi_1(x_1)\psi_2(x_2) + \psi_1(x_2)\psi_2(x_1)\right) \end{aligned}$$

and the antisymmetrized state

$$\begin{aligned} \psi_A(x_1, x_2) &= A\psi_1(x_1)\psi_2(x_2) \\ &= \tfrac{1}{\sqrt{2}} \left(\psi_1(x_1)\psi_2(x_2) - \psi_1(x_2)\psi_2(x_1)\right). \end{aligned}$$

The quantum Liouville equation is given by

$$i\frac{\partial \hat{\rho}}{\partial t} = [\hat{H}, \hat{\rho}].$$

Since the Hamiltonian is always a symmetric function of the dynamic variables, as must be the case for all observables, $\hat{H}$ commutes with all members of the permutation group, that is,

$$[P_i, \hat{H}] = 0.$$

Multiplying the QLE on the left and right by A and A^*, respectively, obtains

$$\begin{aligned} i\frac{\partial A\hat{\rho}A^*}{\partial t} &= A[\hat{H}, \hat{\rho}]A^* \\ &= A\hat{H}\hat{\rho}A^* - A\hat{\rho}\hat{H}A^* \\ &= \hat{H}A\hat{\rho}A^* - A\hat{\rho}A^*\hat{H} \end{aligned}$$

or

$$\frac{\partial \hat{\rho}_A}{\partial t} = -i[\hat{H}, \hat{\rho}_A],$$

where

$$\hat{\rho}_A = A\hat{\rho}A^* = |\Psi_A\rangle\langle\Psi_A|$$

with

$$|\Psi_A\rangle = A|\Psi\rangle.$$

[1] V. G. J. Stoks, R. A. M. Klomp, C. P. F. Terheggen, and J. J. deSwart, Phys. Rev. C **49**, 2950 (1994).
[2] R. B. Wiringa, V. G. J. Stoks, and R. Schiavilla, Phys. Rev. C **51**, 38 (1995).
[3] R. Machleidt, Phys. Rev. C **63**, 024001 (2001).
[4] J. Holz and W. Glockle, Phys. Rev. C **37**, 1386 (1988).
[5] V. N. Kondratyev, A. Bonasera, and A. Iwamoto, Phys. Rev. C **61**, 044613 (2000).
[6] M. S. Marinov and B. Segev, Phys. Rev. A **54**, 4752 (1996).
[7] A. Bonasera and A. Iwamoto, Phys. Rev. Lett. **78**, 187 (1997).
[8] A. Smerzi, V. N. Kondratyev, and A. Bonasera, Nucl. Phys. **A583**, 333 (1995).
[9] E. Wigner, Phys. Rev. **40**, 749 (1932).
[10] E. A. Remler, Ann. Phys. (NY) **95**, 455 (1975).
[11] E. A. Remler, Ann. Phys. (NY) **202**, 351 (1990).
[12] A. Bonasera, V. N. Kondratyev, A. Smerzi, and E. A. Remler, Phys. Rev. Lett. **71**, 505 (1993).
[13] S. John and E. A. Remler, Ann. Phys. (NY) **180**, 152 (1987).
[14] S. John and J. W. Wilson, Phys. Rev. E **49**, 145 (1994).
[15] S. John, Database of nucleon-nucleon scattering cross sections by stochastic simulation, NASA SBIR Phase I Final Report (unpublished) (2005).
[16] S. John, L. W. Townsend, J. W. Wilson, and R. K. Tripathi, Phys. Rev. C **48**, 766 (1993).
[17] E. A. Remler, private communication (NSF report) (1993).
[18] J. W. Wilson *et al*. NASA RP-1257 (1991).